frontiers | Frontiers in Marine Science

TYPE Original Research
PUBLISHED 07 February 2023
DOI 10.3389/fmars.2023.1101095

OPEN ACCESS

EDITED BY
Ravi Bhushan,
Physical Research Laboratory, India

REVIEWED BY
Frank Dehairs,
Vrije University Brussels, Belgium
Wilson Machado,
Fluminense Federal University, Brazil

*CORRESPONDENCE
Florian Scholz
fscholz@geomar.de

SPECIALTY SECTION
This article was submitted to Marine Biogeochemistry, a section of the journal Frontiers in Marine Science

RECEIVED 17 November 2022
ACCEPTED 20 January 2023
PUBLISHED 07 February 2023

CITATION
Scholz F, Cheng J, Zhang Z, Vosteen P, Siebert C and Frank M (2023) Benthic-pelagic coupling and isotopic fractionation of barium in Kiel Bight, SW Baltic Sea. *Front. Mar. Sci.* 10:1101095. doi: 10.3389/fmars.2023.1101095

Benthic-pelagic coupling and isotopic fractionation of barium in Kiel Bight, SW Baltic Sea

Florian Scholz[1]*, Jun Cheng[1,2,3,4], Zhouling Zhang[1], Paul Vosteen[1], Christopher Siebert[1] and Martin Frank[1]

[1]Marine Biogeochemistry, GEOMAR Helmholtz Centre for Ocean Research Kiel, Kiel, Germany, [2]Fourth Institute of Oceanography, Ministry of Natural Resources, Beihai, China, [3]Key Laboratory of Ocean and Marginal Sea Geology, South China Sea Institute of Oceanology, Chinese Academy of Sciences, Guangzhou, China, [4]University of Chinese Academy of Sciences, Beijing, China

Barium (Ba) isotopes are a promising new tracer for riverine freshwater input to the ocean and marine biogeochemical cycling. However, many processes that affect Ba cycling at continental margins have not yet been investigated with respect to Ba isotope fractionation. Here, we present a comprehensive data set of Ba concentration and isotope data for water column, pore water and sediment samples from Kiel Bight, a seasonally stratified and hypoxic fjord in the southwestern Baltic Sea. The surface water Ba concentration and Ba isotope inventory of the water column can generally be explained by mixing of riverine freshwater and Atlantic seawater. However, the deep-water below the seasonal pycnocline (10 - 15 m water depth) is characterized by a pronounced positive Ba concentration anomaly (up to 915 nM) that is accompanied by a δ^{138}Ba of ~+0.25 ‰, which is lighter than expected from the seawater-freshwater mixing line (Ba: 77 nM, δ^{138}Ba: +0.32 ‰ at a salinity of 18). Pore water profiles indicate a Ba flux across the sediment-water interface, which contributes to the enrichment in isotopically light Ba in the deep-water. Pore waters of surface sediments and deep-waters are oversaturated with respect to barite. Therefore, barite dissolution is unlikely to account for the benthic Ba flux. Water column Ba concentrations closely correlate with those of the nutrients phosphate and silica, which are removed from surface waters by biological processes and recycled from the sediment by diffusion across the sediment-water interface. As nutrient-to-Ba ratios differ among sites and from those observed in open-marine systems, we propose that Ba is removed from surface waters by adsorption onto biogenic particles (rather than assimilation) and regenerated within surface sediments upon organic matter degradation. Pore water data for subsurface sediments in Kiel Bight indicate preferential transfer of isotopically heavy Ba into an authigenic phase during early diagenesis. Quantifying the burial flux associated with this authigenic Ba phase along continental margins could potentially help to settle the isotopic imbalance between known Ba source and sink fluxes in the ocean.

KEYWORDS

barium isotopes, sediment, pore water, benthic flux, early diagenesis

1 Introduction

Dissolved Ba in open-ocean seawater shows a nutrient-like distribution (Chan et al., 1977) and the amount of particulate Ba sinking through the water column as biogenic barite ($BaSO_4$) has been shown to be correlated to carbon export from the surface ocean (Dymond et al., 1992; Dymond and Collier, 1996). As a consequence of these general observations, numerous studies have attempted to use Ba concentrations and fluxes or barite abundances in sediments as a proxy for marine primary or export productivity (e.g., Paytan et al., 1996; Nürnberg et al., 1997; Paytan and Griffith, 2007). More recently, isotope measurements of dissolved Ba in seawater from most major ocean basins have highlighted the potential of Ba isotopes to identify and disentangle the processes that contribute to the vertical and horizontal distribution of Ba in the ocean (Horner et al., 2015; Cao et al., 2016; Bates et al., 2017; Hsieh and Henderson, 2017; Bridgestock et al., 2018; Horner and Crockford, 2021; Whitmore et al., 2022). Further research on Ba isotope fractionation during water-solid interactions in different marine systems is, however, required to fully explore the utility of Ba isotopes as a (paleo-)biogeochemical tracer.

Despite the nutrient-like behavior of Ba in the water column and unlike essential nutrients such as nitrogen, phosphorus and iron, Ba is not required for cellular processes. However, culture experiments suggest that planktonic organisms (Fisher et al., 1991) and bacterial biofilms (Martinez-Ruiz et al., 2018) can take up dissolved Ba from seawater, which is subsequently partly released during organic matter remineralization (Ganeshram et al., 2003). Upon downward sinking of organic particles into the mesopelagic zone (200 - 600 m water depth), Ba becomes enriched in organic matter-rich micro-niches and precipitates in the form of barite even though the surrounding seawater is undersaturated with respect to barite (Dehairs et al., 1980; Bishop, 1988). Due to this undersaturation, a significant fraction of the pelagic barite subsequently dissolves during sinking through the water column or in surface sediments and is not buried (Church and Wolgemuth, 1972; Paytan and Kastner, 1996; McManus et al., 1998).

Barium isotope analyses of pelagic barite and barite from precipitation experiments suggest that the light Ba isotopes are preferentially incorporated into barite (von Allmen et al., 2010; Horner et al., 2017; Crockford et al., 2019). This notion is consistent with the observation that Ba depleted surface waters are generally characterized by a higher δ^{138}Ba than Ba replete deep-waters (Horner et al., 2015; Hsieh and Henderson, 2017). In addition, large lateral differences in δ^{138}Ba are observed throughout the ocean (overall range of $\delta^{138}Ba_{seawater}$ between +0.2 and +0.65 ‰), which is thought to be mainly caused by progressive removal of isotopically light Ba from surface waters and remineralization in deep-waters along the global thermohaline circulation (Bates et al., 2017; Hsieh and Henderson, 2017; Horner and Crockford, 2021).

At the ocean margins, Ba is supplied to seawater from the continents *via* river runoff (Elderfield and Schultz, 1996) and submarine groundwater discharge (Shaw et al., 1998). During chemical weathering, some of the Ba mobilized from crustal material is adsorbed to secondary minerals such as iron (Fe) and manganese (Mn) oxides or clay minerals. Given that the light Ba isotopes are preferentially adsorbed (Gong et al., 2020), river water is generally characterized by higher δ^{138}Ba (+0.1 to +0.35 ‰) (Cao et al., 2016; Bridgestock et al., 2021a; Bridgestock et al., 2021b; Cao et al., 2021) than crustal rocks (0.0 ± 0.03 ‰) (Nan et al., 2018) but a lower δ^{138}Ba than seawater. Dissolved Ba concentrations in rivers are generally higher than those in seawater (Rahman et al., 2022) and additional Ba is released from riverine particles by ion exchange during estuarine mixing (Hanor and Chan, 1977; Coffey et al., 1997; Bridgestock et al., 2021a). The differences in river water and seawater Ba concentrations and isotope compositions have been proposed as a (paleo-)proxy for freshwater input (Bridgestock et al., 2021b; Yu et al., 2022 and references therein).

By the current state of research, the global ocean's Ba isotope budget is not balanced since the main Ba input *via* river runoff has a higher δ^{138}Ba than pelagic barite (~0 ‰), which is considered the main Ba sink. Some of this imbalance could be explained by desorption of isotopically light particulate Ba (with a δ^{138}Ba ~0.2 ‰ lower than river water) within the estuarine mixing gradient (Bridgestock et al., 2021a). In addition, other Ba sources and sinks, which have not yet been characterized isotopically, could potentially close the oceanic Ba mass balance: Water column studies suggest that another important external flux of Ba to the ocean originates from the seafloor (Rahman et al., 2022; Whitmore et al., 2022). It is well established that marine sediments release Ba to the bottom water *via* diffusion or advection across the sediment-water interface (McManus et al., 1994; Paytan and Kastner, 1996; McManus et al., 1998). Among the processes potentially contributing to this flux are barite dissolution and release of Ba from metal oxides or organic material. Benthic Ba sources are likely particularly relevant at continental margins where the surface ocean and seafloor are close to each other and where high rates of terrigenous and biogenic sedimentation prevail. The isotopic composition of the benthic Ba flux and mechanisms of isotope fractionation during pore water-sediment interactions in such settings have not been studied systematically so far.

We investigated the coupling of sedimentary and water column Ba cycling in Kiel Bight in the western Baltic Sea. Due to seasonal stratification and anthropogenic eutrophication (Wasmund et al., 2008; Maar et al., 2016), Kiel Bight is characterized by steep seasonal redox gradients in the water column and sediments (Dale et al., 2013; Lennartz et al., 2014). Furthermore, the residence time of the deep-waters (~1 month in the summer) (Dietze and Löptien, 2021) is long enough to allow sedimentary Ba fluxes to generate a traceable signal in the bottom water yet short enough to allow vertical mixing of deep-water and surface water and the associated mechanism of Ba isotope fractionation to be studied as well. Kiel Bight is therefore considered a natural laboratory where the influence of sedimentary processes on the Ba isotope composition of coastal and near bottom seawater can be evaluated.

2 Study area

The Baltic Sea is a semi-restricted marginal sea in Northern Europe, which is connected to the North Sea *via* the narrow and shallow Danish straits (Figure 1). Due to limited water exchange though these straits and a positive freshwater balance in the drainage area, Baltic seawater is brackish with surface water salinities decreasing from ~20 in the Danish straits to <1 in the Bothnian

10.3389/fmars.2023.1101095

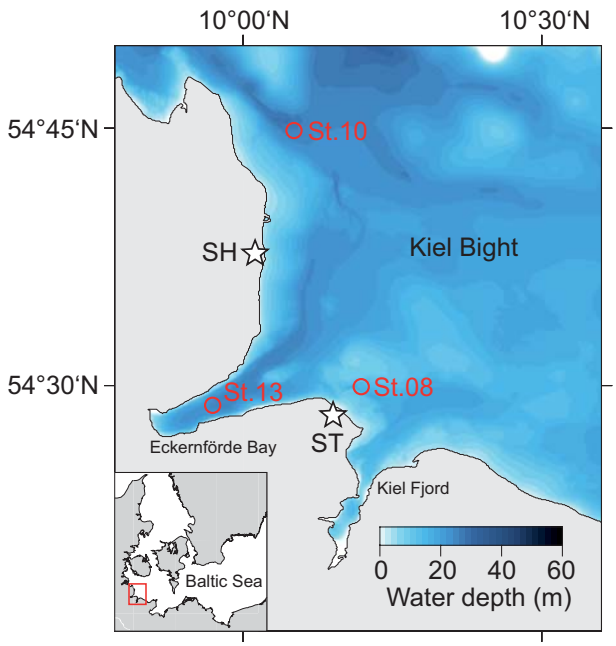

FIGURE 1
Bathymetric map of Kiel Bight within the western Baltic Sea (see inlet) showing the sampling locations in Kiel Bight (circles) and at coastal cliffs (stars; SH, Schönhagen; ST, Stohl).

Bay at the northeastern end of the basin. During irregular large inflow events, fully saline and well–oxygenated water from the North Sea is transported into the basin, which affects the hydrography and redox conditions in the Baltic Sea (Matthäus et al., 2008; Mohrholz et al., 2015; Dellwig et al., 2018; Mohrholz, 2018; Scholz et al., 2018).

Kiel Bight is a sub-basin of the southwestern Baltic Sea (Figure 1). It is bounded to the south and west by the German coast of Schleswig-Holstein and the narrow Kiel Fjord and Eckernförde Bay, and to the north by the Danish islands. Kiel Bight is characterized by a complex seafloor topography that includes shallow moraine shoals and deeper narrow basins, channels and depressions, which were formed by the Scandinavian Ice Sheet during the Last Glacial. The surrounding coastal cliffs consist of glacial till and retreat by decimeters to meters each year, mainly in winter due to erosion during storm events (Averes et al., 2021). The lithogenic and pedogenic material contained in the glacial till (feldspar, quartz, mica, clay minerals and Fe oxides) is transferred into Kiel Bight by surface runoff and wave action and represents the predominant source of terrigenous sediments (Seibold et al., 1971). Coarse grained sediment particles are retained near-shore whereas the fine-grained fraction is transported over longer distances and accumulates in deeper channels and basins (Seibold et al., 1971). The glacial till also contains up to 30% of calcium carbonate (Averes et al., 2021), which is mostly dissolved due to undersaturation in the bottom water and pore waters of surface sediments (Wallmann et al., 2022).

The hydrographic setting in Kiel Bight is subject to pronounced seasonal variability (Lennartz et al., 2014). From November until March, the water column is characterized by almost homogenous temperatures. A thermocline separating laterally well-mixed surface waters from spatially restricted deep-waters usually develops in April at 10 to 15 m water depth and persists until October. Even though a halocline is present in the water column throughout the year, the strongest salinity gradients are observed from April to October. High primary productivity in surface waters from late spring through fall causes intense export of organic matter (Wasmund et al., 2008; Maar et al., 2016), which is remineralized in the deep-water and surface sediment leading to hypoxic (<63 µM of O_2) to anoxic, and locally even sulfidic conditions. By late fall, stratification in the water column is weakened by wind-induced vertical mixing leading to re-oxygenation of the deep-water (Lehmann and Myrberg, 2008; Lennartz et al., 2014). Redox conditions in the fine-grained surface sediments in the deeper areas of Kiel Bight vary between manganous or ferruginous and sulfidic. The most reducing conditions in surface sediment are generally observed in late summer and fall (Dale et al., 2013).

Water and sediment samples were collected at three sites in the Kiel Bight during R/V Alkor Cruise AL543 (Figure 1; Table 1). Station 8 is located in a near-shore depression separated from the open Kiel Bight in three directions by shallow moraine shoals. Station 10 is located within the channel connecting the deeper areas of Kiel Bight to the Danish straits. Station 13 is located within Eckernförde Bay at the landward end of this same channel. Bathymetric restriction of the deep-water increases from Station 10 to Station 13 to Station 8 (Dietze and Löptien, 2021).

3 Materials and methods

3.1 Sampling

RV Alkor Cruise AL543 took place in August 2020. The geographical positions and water column properties of all sampling stations are provided in Table 1. Water column samples and temperature and salinity data were obtained by deploying a HydroBIOS MWS 12 rosette water sampler equipped with a CTD. A novel trace metal-clean bottom water sampler (Benthic Trace Profiler) (Plass et al., 2022) was also

TABLE 1 Geographical coordinates, water depth and general properties of the sampling stations.

Staion	Longitude (deg E)	Latitude (deg N)	Water depth (m)	DW[a] salinity	DW[a] oxygen (µM)	BW[b] H_2S (µM)	Mean TOC[c] (wt.%)
8	10°11'	54°29'	23.0	19.9	<LD[d]	53	3.4 ± 1.4 (12)
10	10°05'	54°45'	26.0	21.6	31	0	5.2 ± 0.6 (13)
13	9°57'	54°29'	25.7	19.2	80	5	5.3 ± 1.5 (13)

[a]DW (deep water) refers to the deepest CTD measurement.
[b]BW (bottom water) refers to the water overlying the sediment in the MUC liner.
[c]Average TOC ± SD (number of samples) in the recovered depth interval.
[d]<LD: Below limit of detection (<2 µM O_2).

deployed at Station 8 to collect waters close to the seafloor. Short sediment cores were retrieved together with the overlying bottom water using a mini multiple corer (MUC). The sediment cores were transferred to the home laboratory for subsampling and pore water recovery (see Scholz et al. (2011) for details). The bottom water was siphoned off with a tube and subsequently treated like pore water samples. Sediments were sub-sampled in an argon-flushed glove bag by cutting the core into 1 - 4 cm thick slices with the highest resolution at the surface. The pore water was separated from the solid phase by centrifuging for 20 minutes at 4000 rpm. The supernatant water was filtered through 0.45 µm cellulose acetate syringe filters and split into several aliquots for the determination of Fe^{2+}, H_2S, anion and metal concentrations. Aliquots for the metal analyses were stored in acid-cleaned LDPE vials and acidified with concentrated HNO_3 (sub-boiling distillation). A wet sediment aliquot was stored in air tight pre-weighed plastic cups for the determination of water content and porosity followed by total digestion for element and isotopic analyses. As the main source of sediments to Kiel Bight is coastal erosion (see above), we also analyzed solid phase samples taken at the most prominent coastal cliffs in Stohl and Schönhagen (Figure 1) to determine the regional terrigenous background ratio of Ba to aluminum (Al) and $\delta^{138}Ba$.

3.2 Chemical analyses

Dissolved O_2 concentrations in the water column were determined by Winkler titration. The seawater samples for dissolved nutrient analysis (NO_3^-, PO_4^{3-} and SiO_4^{4-}) were filtered through 0.2 µm PES-filters and stored frozen in polypropylene bottles until analysis in the shore-based laboratories using a Quaatro Seal Autoanalyser. Concentrations of NH_4^+, PO_4^{3-}, SiO_4^{4-} and Fe^{2+} in bottom water and pore water samples were analyzed by standard spectrophotometric techniques (Stookey, 1970; Grasshoff et al., 1999). Hydrogen sulfide ($\Sigma H_2S = H_2S + HS^- + S^{2-}$) concentrations in the water column and pore waters were also determined photometrically by applying the methylene blue method (Grasshoff et al., 1999). Bottom water and pore water SO_4^{2-} concentrations were analyzed by ion chromatography. The concentrations of Ba and Mn in the water column and pore waters were determined by inductively coupled plasma optical emission spectroscopy (ICP-OES, VARIAN 720-ES) and inductively coupled plasma mass spectrometry (ICP-MS, Agilent Technologies 7500 Series).

The total organic carbon (TOC) content of freeze-dried and ground sediment samples was determined with an element analyzer (Euro EA, HEKAtech). For the analysis of total element concentrations, ~100 mg of freeze dried and ground sediment samples and coastal cliff samples were digested in HF (40%, supra pure), HNO_3 (65%, supra pure) and $HClO_4$ (60%, p.a.) on a hotplate and the resulting solutions were analyzed by ICP-OES. The accuracy of the digestion procedure was monitored by inclusion of method blanks and the reference standards PACS-3 (marine sediment, Canadian Research Council), MESS-3 (Marine Sediment Reference Material, Canadian Research Council) as well as the in-house standard OMZ-2. Average values of replicate digestions were generally well within the recommended ranges with relative standard deviations (RSD) being <1% for Al and <2% for Ba (n=5).

Ba isotope compositions were measured using a double spike (^{130}Ba-^{135}Ba) technique (Yu et al., 2020), which was modified from the one of Horner et al. (2015). Aliquots containing ~50 ng Ba were taken from seawater, pore waters and total sediment digestions for the determination of Ba isotope compositions. Note that due to limited volumes of seawater samples from the CTD casts, samples from the shallow water column with low Ba concentrations had to be combined to obtain enough Ba for isotope analyses. In brief, appropriate quantities of the ^{130}Ba-^{135}Ba double spike solution were equilibrated with sample aliquots on a hotplate at 80°C for at least 24 hours. A pre-treated Ba-free Na_2CO_3 solution was added stepwise to seawater samples to co-precipitate Ba with $CaCO_3$. The resulting precipitate was centrifuged and dissolved in 1 mL 1 M HCl. The water and total digestion samples were evaporated and then re-dissolved in 1 mL 1 M HCl. Chemical separation was performed twice using cation exchange resin (AG50W-X8, 200-400 mesh, 1.4 mL volume). The matrix elements were first eluted with 8 mL of 1 M HCl and 8 mL of 3 M HCl, followed by collection of Ba with 10 mL of 2 M HNO_3. Finally, the Ba cut was evaporated and dissolved in 2% (v/v) HNO_3 for Ba isotope analyses. Ba isotope analyses were conducted at GEOMAR Helmholtz Centre for Ocean Research Kiel using a Neptune Plus (Thermo Finnigan) MC-ICP-MS. The purified sample solutions were introduced as a dry aerosol using an Aridus II desolvator system and an Aspire PFA micro-concentric nebulizer (uptake rate of ~50 µL min^{-1}). Tuning for an appropriate Normalized Ar Index (NAI; an index of plasma temperature) prior to measurement attenuated possible matrix effects (Yu et al., 2020). The geometrical procedure described in Siebert et al. (2001) was used for data reduction. Each sample solution was analyzed three to five times in two different measurement sessions, with external sample reproducibilities between ±0.01 and ±0.07 ‰ (2SD). Long term repeated measurement of reference materials at GEOMAR over a course of three years yield $\delta^{138}Ba_{NIST}$ values of +0.62 ± 0.03 ‰ (2 SD, n = 6) and 0.29 ± 0.03 ‰ (2 SD, n = 19) for seawater reference samples SAFe surface and SAFe 1000 m, respectively, and 0.29 ± 0.03‰ (2 SD, n = 27) for carbonate reference material JCP, which are all within error identical to those reported by three other laboratories (Hsieh and Henderson, 2017; Geyman et al., 2019; Cao et al., 2021). Long term measurements of in-house seawater reference samples BATS 15 m and 2000 m also show similar reproducibility: 0.55 ± 0.05 ‰ (2 SD, n = 26) and 0.47 ± 0.04 ‰ (2 SD, n = 18) respectively. The Ba isotope compositions are reported as $\delta^{138}Ba$ values relative to the Ba SRM NIST3104a:

$$\delta^{138}\mathbf{Ba} = \left(\frac{^{138/134}\mathbf{Ba}_{\mathbf{sample}}}{^{138/134}\mathbf{Ba}_{\mathbf{NIST3104a}}} - \mathbf{1}\right) \cdot \mathbf{1000} \quad (1)$$

3.3 Calculation of benthic fluxes

Benthic diffusive fluxes (F) across the benthic boundary were calculated applying Fick's first law of diffusion (Schulz, 2006):

$$\mathbf{F} = -\phi \cdot \mathbf{D}_{\mathbf{sed}} \cdot \frac{\mathbf{d[C]}}{\mathbf{dx}} \quad (2)$$

In Eq. 2, ϕ is porosity, D_{sed} is the diffusion coefficient of ions in sediment and d[C]/dx denotes the ion concentration gradients between the uppermost pore water sample (0 – 1 cm) and the overlying bottom water. Negative values indicate a flux from the pore water into the bottom water and positive values represent a flux

from the bottom water into the pore water. The diffusion coefficients of ions in seawater (D_{sw}) under standard conditions (Li and Gregory, 1974) were adjusted to *in situ* temperature, pressure and salinity applying the Stokes-Einstein equation. Diffusion coefficients of ions in sediments (D_{sed}) were calculated from the diffusion coefficients in seawater (D_{sw}) taking into account tortuosity (θ_2):

$$D_{sed} = \frac{D_{sw}}{\theta^2} \quad (3)$$

Tortuosity was calculated from porosity using the following relationship from Boudreau (1996):

$$\theta^2 = 1 - \ln(\phi^2) \quad (4)$$

3.4 Calculation of saturation indexes

The saturation index (SI) for barite in the water column and sediment pore waters was calculated applying the geochemical model PHREEQC by Parkhurst and Appelo (2013) using the PHREEQC data base. Saturation indexes greater than 0 indicate that aqueous solutions were oversaturated with respect to barite whereas SIs below 0 indicate undersaturation with respect to barite and potential barite dissolution. A saturation index close to 0 indicates that dissolution and precipitation of barite reached equilibrium. Input data of the chemical equilibrium calculations include temperature, alkalinity and concentrations of all major ions in seawater (including SO_4^{2-}) and Ba^{2+}.

4 Results

4.1 Water column

During Cruise AL543 in August 2020, temperature and salinity in the upper water column (above 10 - 15 m) ranged from 18.1 to 19.4°C and from 14.7 to 16.8, respectively (Figures 2A, B). Below this depth range, temperature dropped and salinity increased sharply with depth, ranging from 13.5 to 18.3°C and from 16.4 to 21.6, respectively. The temperature and salinity profiles reflect pronounced pycnoclines and are consistent with stable stratification of the water column during late summer (Lennartz et al., 2014). The pycnocline was shallower at Station 8 (~8 m depth; roughly corresponding to the depth of the surrounding moraine shoals) and deeper at Stations 10 and 13 (~15 m depth). Dissolved O_2 concentrations were high in surface waters (~250 µM) and dropped sharply below 7 m depth. The deepest samples at Stations 10 and 13 were still oxic (O_2 concentrations of 31 µM and 80 µM, respectively). The deep-water at Station 8 was anoxic below ~15 m depth (Figure 2C). The concentrations of SiO_4^{4-} and PO_4^{3-} were low in the upper water column above the pycnocline and increased sharply below (Figures 2D, E). In contrast, NO_3^- concentrations were low throughout the water column, except for somewhat elevated concentrations in the bottom water at Stations 8 and 10 (Figure 2F). The deep-water was thus characterized by a nitrate deficit relative to phosphate when compared to the average nitrogen to phosphorus ratio in phytoplankton (Redfield ratio), as indicated by a negative N* ($N^* = NO_3^- - 16 \cdot PO_4^{3-}$) (Gruber and Sarmiento, 1997) (Figure 2G).

At Station 8, dissolved Mn concentrations increased below 10 m water depth and reached maximum concentrations of ~12 µM in the deep-water. Hydrogen sulfide concentrations up to ~45 µM were detected in the deep-water at Station 8 (Figure 2H). In contrast, at Stations 10 and 13 dissolved Mn concentrations varied little and remained below 1.2 µM throughout the water column (Figure 2I). Above the pycnocline, dissolved Ba concentrations were relatively constant between 41 and 116 nM at all stations. Below the pycnocline, dissolved Ba concentrations were higher and ranged from 147 to 938 nM. The highest dissolved Ba concentrations were observed in the deep-water of Station 8 (Figure 2J). Seawater above the pycnocline was undersaturated with respect to barite ($SI_{Barite} < 0$), whereas the deep-water was oversaturated ($SI_{Barite} > 0$) (Figure 2K).

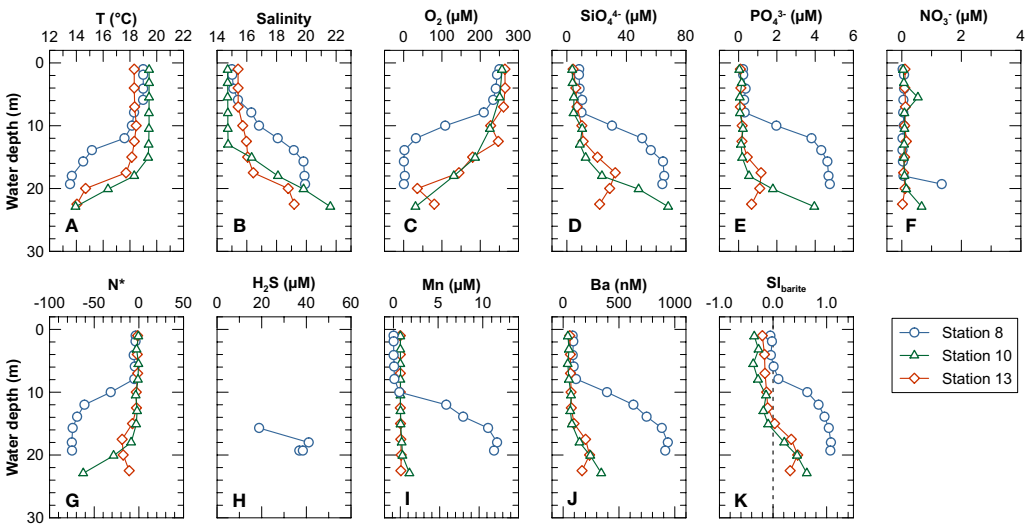

FIGURE 2
Depth profiles of **(A)** temperature, **(B)** salinity, **(C)** dissolved O_2, **(D)** SiO_4^{4-}, **(E)** PO_4^{3-}, **(F)** NO_3^-, **(G)** N* ($N^* = NO_3^- - 16 \times PO_4^{3-}$), **(I)** Mn, **(J)** Ba and **(K)** saturation index for barite in the water column. Note that **(H)** shows H_2S in the deep water close to the seafloor at Station 8 sampled using the Benthic Trace Profiler.

4.2 Sediment pore water

Pore water dissolved Mn profiles were characterized by a peak within the upper 5 cm of the sediment (12.8 - 70.6 µM) and decreased (Stations 8 and 13) or increased again (Station 10; up to 126.5 µM) towards the lower end of the core (Figure 3A). Pore water dissolved Fe concentrations were high (up to ~48 µM) in the uppermost 3 cm at Station 10 but low throughout the profiles at the other two stations (Figure 3B). Pore water SO_4^{2-} concentrations decreased (Figure 3C) and those of H_2S, NH_4^+, PO_4^{3-} and SiO_4^{4-} increased with depth at all three stations (Figures 3D–G). The pore waters at Station 13 were more depleted in SO_4^{2-} (approaching zero at the lower end of the core) and more enriched in H_2S and NH_4^+ than at Stations 8 and 10.

Pore water dissolved Ba concentrations reached a maximum in the uppermost 1 or 2 cm of the sediment column and decreased sharply below (Figure 3H). At Stations 8 and 10 pore water Ba concentrations remained essentially constant below 5 cm sediment depth. In contrast, at Station 13, dissolved Ba concentrations increased again below 4 cm depth and reached ~1000 nM at the lower end of the core (Figure 3H). Bottom waters and pore waters above 4 cm were oversaturated with respect to barite at all three stations, especially at the depths corresponding to the dissolved Ba maximum (SI_{barite} up to 0.80). Below 4 cm, most pore waters were close to equilibrium with respect to barite ($0.05 \leq SI_{Barite} \leq 0.30$) (Figure 3I). At Station 13, the pore water were undersaturated with respect to barite below 18 cm depth ($SI_{Barite} < 0$) (Figure 3I), coincident with decreasing sulfate but increasing dissolved Ba and H_2S concentrations (Figures 3C, D, H).

The concentrations of PO_4^{3-}, SiO_4^{4-}, H_2S, NH_4^+, Fe, Mn and Ba in the uppermost pore water samples (0.5 cm) were higher than their respective concentrations in the overlying bottom water (0.0 cm) (except H_2S at Station 10 and Fe^{2+} at Station 8). These concentration gradients across the sediment-water interface are indicative of a diffusive flux of these solutes from the sediments into the bottom water (Table 2).

4.3 Sediment solid phase

Solid phase Ba, Al and TOC concentrations were corrected for the amount of salt and pore water Ba that was transferred to the solid phase upon freeze drying (based on water content, pore water salinity and Ba concentrations). At all three stations, the concentrations of Ba and Al were lowest in the uppermost sediment layer (0 - 1 cm). Below the surface sediment, corrected Ba concentrations in the sediment ranged from 315 µg g^{-1} to 416 µg g^{-1} and bulk Al concentrations varied between 30.1 mg g^{-1} and 57.0 mg g^{-1}, both remaining essentially constant with depth (Figure 4). The coastal cliff material had an average Ba

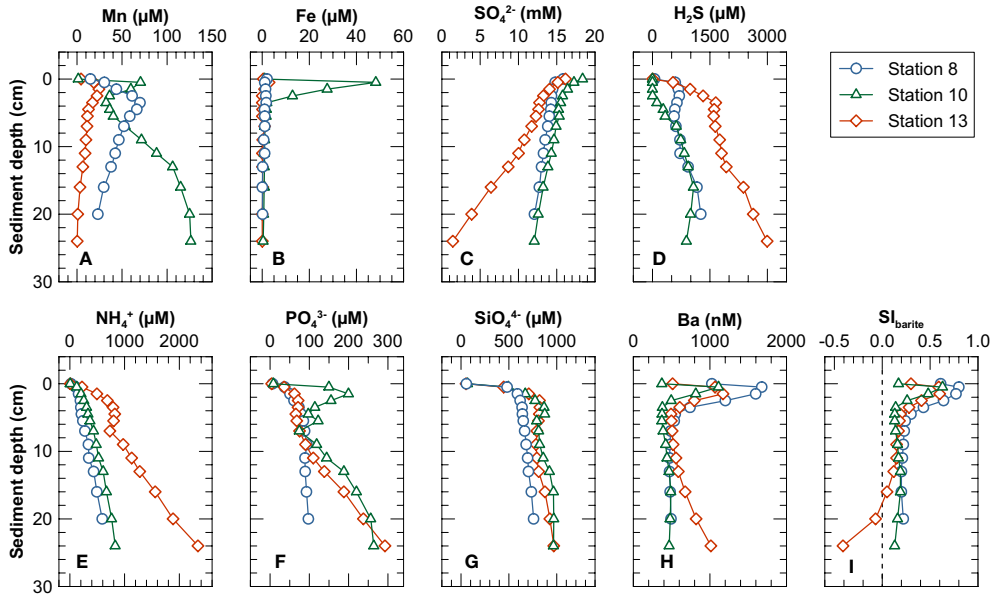

FIGURE 3
Pore water profiles of **(A)** Mn, **(B)** Fe, **(C)** SO_4^{2-}, **(D)** H_2S, **(E)** NH_4^+, **(F)** PO_4^{3-}, **(G)** SiO_4^{4-}, **(H)** Ba and **(I)** saturation index for barite. The uppermost sample in each profile (depth of 0.0 cm) represents the bottom water overlying the sediment in the MUC liners.

TABLE 2 Diffusive fluxes (in µmol cm^{-2} yr^{-1}) across the sediment-water interface.

Station	PO_4^{3-}	SiO_4^{4-}	H_2S	NH_4^+	Fe	Mn	Ba
8	-8.20	-198	-406	-73	0.29	-4.6	-0.24
10	-37.2	-195	0.0	-100	-14.4	-20.2	-0.27
13	-8.70	-187	-406	-188	-0.79	-4.3	-0.21

concentration of 332 ± 38 μg g^{-1} and a Ba/Al of 0.010 ± 0.002 (SD, n = 36). Pore water corrected Ba/Al ratios of the uppermost sediment samples at Stations 8 and 13 exceeded this regional background ratio, while the ratios of other sediment core samples were lower than the regional terrigenous background value (Figure 4). Organic carbon concentrations were highest in the uppermost sediment intervals (up to 8.7 wt.%) and decreased with depth (Figure 4).

4.4 Barium isotope data

Above the pycnocline, where dissolved Ba concentrations were low, the seawater δ^{138}Ba values varied little with depth and ranged from +0.36 ‰ to +0.42 ‰ (Figure 5). Below the pycnocline at Stations 8 and 10, where dissolved Ba concentrations increased, the δ^{138}Ba was generally lower than in the surface waters (average of +0.28 ± 0.04 ‰, n = 9). Below the pycnocline at Station 13, seawater δ^{138}Ba also decreased at first but then increased again (average of +0.35 ± 0.04 ‰, n = 4). Dissolved Ba and δ^{138}Ba distributions in the water column display a mirror image with high dissolved Ba concentrations corresponding to low δ^{138}Ba values (Figure 5).

The dissolved Ba concentration maximum at the sediment surface was characterized by a δ^{138}Ba similar to that in the overlying bottom and deep-water (Figure 5). Below the concentration maximum at the sediment surface, pore water δ^{138}Ba first decreased within the upper few centimeters and then either remained constant (Stations 8 and

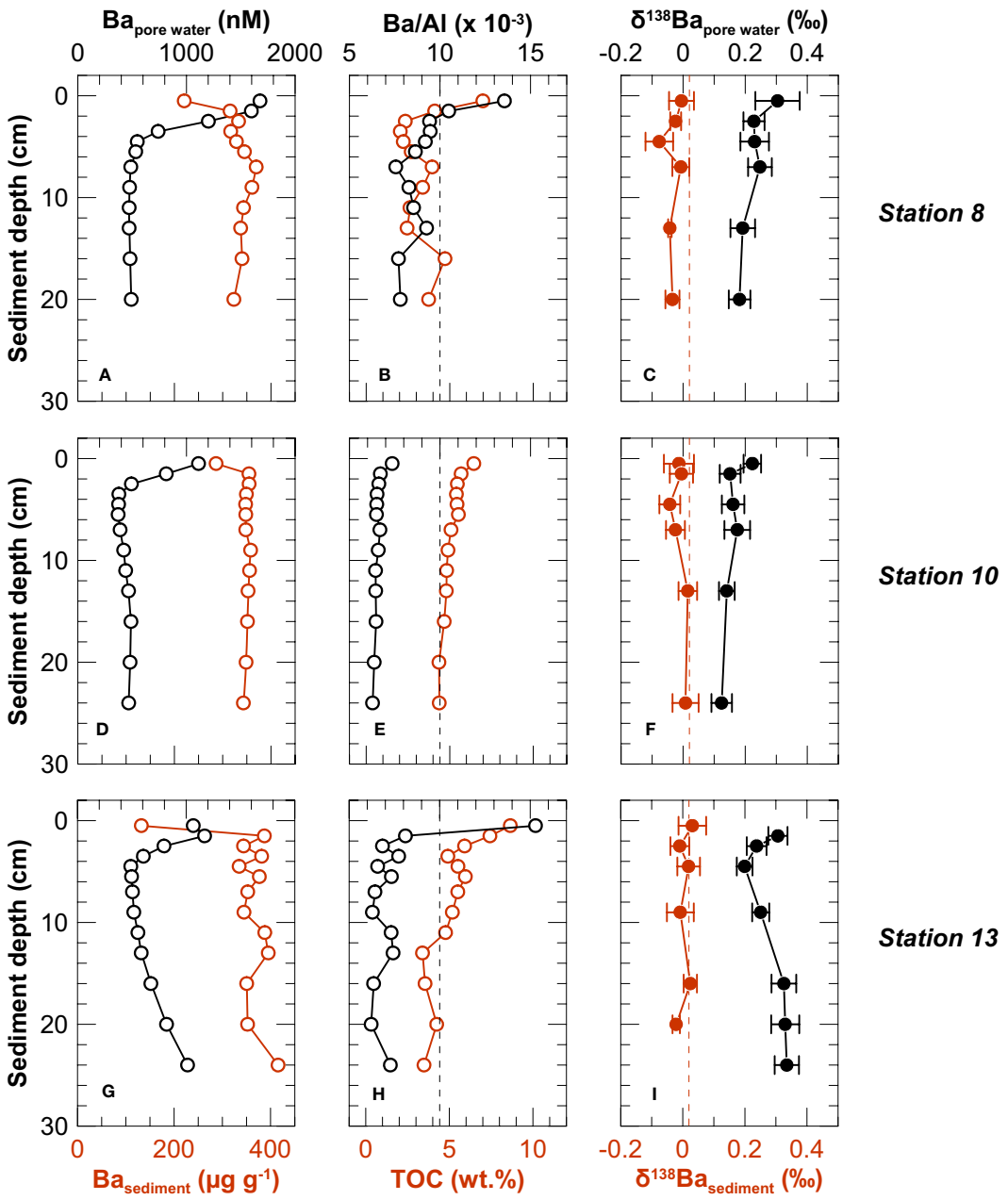

FIGURE 4
Depth profiles of Ba concentrations in the pore water and sediments (left column: **A**, **D**, **G**), Ba/Al and TOC in sediments (central column: **B**, **E**, **H**), and δ^{138}Ba of pore water and sediments (right column: **C**, **F**, **I**). Vertical lines in the central and right column represent the average Ba/Al (black) and δ^{138}Ba (red) of coastal cliffs.

10) or increased again to reach +0.34 ‰ at Station 13, coincident with downcore increasing Ba concentrations (Figure 5). Unlike in the water column, dissolved Ba and δ^{138}Ba distributions in the pore water did not display a mirror image. Instead, the highest Ba isotope values coincided with high dissolved Ba concentrations at Station 13 (Figure 5). The δ^{138}Ba values of solid phase samples are uniform within analytical error (-0.01 ± 0.03‰, SD, n = 18) (Figure 4) and identical to the δ^{138}Ba of the terrigenous sediment source from the coastal cliffs (+0.02 ± 0.03, SD, n = 6).

5 Discussion

5.1 Freshwater-seawater mixing within Kiel Bight

Baltic Sea water is generated by mixing of freshwater from the Baltic Sea drainage area and North Atlantic seawater entering *via* the Danish straits. Freshwater is generally characterized by higher Ba concentrations and a lower δ^{138}Ba than seawater (e.g., Cao et al., 2016; Cao et al., 2020; Bridgestock et al., 2021a; Bridgestock et al., 2021b; Rahman et al., 2022). Therefore, it is likely that the Ba concentration and isotopic distribution in Kiel Bight is to some extent a function of mixing of freshwater and seawater.

The dissolved Ba concentration and isotope composition resulting from mixing of freshwater and seawater are given by the following equations:

$$[Ba]_{mix} = f_{fresh} \cdot [Ba]_{fresh} + f_{sw} \cdot [Ba]_{sw} \quad (5)$$

$$\frac{\delta^{138}Ba_{mix} = f_{fresh} \cdot [Ba]_{fresh} \cdot \delta^{138}Ba_{fresh} + f_{sw} \cdot [Ba]_{sw} \cdot \delta^{138}Ba_{sw}}{[Ba]_{mix}} \quad (6)$$

In Eq. 5 and 6, [Ba] denotes Ba concentrations and f_{fresh} and f_{sw} are the fractions of freshwater and seawater, respectively (f_{fresh} + f_{sw} = 1). Salinity along the estuarine mixing gradient is calculated analogous to Eq. 5. Because no Ba isotope data for rivers entering the Baltic Sea are available, the Ba concentration (116 nM) and δ^{138}Ba (+0.23 ‰) of Eurasian riverine freshwater (Bridgestock et al., 2021b) were used in Eq. 5 and 6. The catchment areas of both the Baltic Sea and Eurasian rivers are located at mid to high northern latitudes thus justifying this choice of δ^{138}Ba for the freshwater end member. The Ba concentration (43 nM) and δ^{138}Ba (+0.53 ‰) of North Atlantic surface seawater (Bridgestock et al., 2021b) was chosen for the seawater end member.

Dissolved Ba concentrations in laterally well-mixed surface waters (S = 15) plot on a mixing line between freshwater and North Atlantic seawater (Figure 6A). In contrast, denser (S = 19.2 - 21.6) and more restricted deep-waters are strongly enriched in dissolved Ba compared to the freshwater-seawater mixing line. The δ^{138}Ba of water column

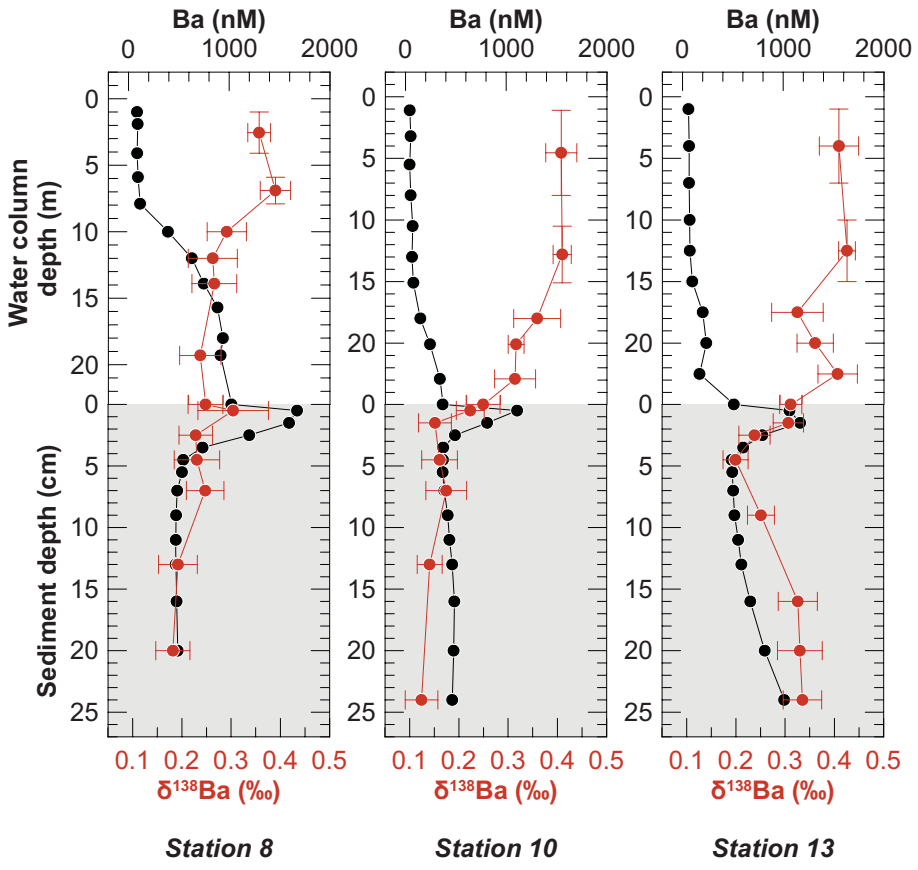

FIGURE 5
Composite depth profiles of Ba concentration (black symbols) and δ^{138}Ba (red symbols) in the water column (white background) and pore water (gray background). Horizontal error bars represent the 2 SD of δ^{138}Ba. The vertical bars in the upper water column represent the depth range over which samples were combined (see Method section 3.2). Note differing y-axes scales in the water column.

samples plot both above and below the mixing relationship between freshwater and North Atlantic seawater (Figure 6B) suggesting that the mean δ^{138}Ba of the water column Ba inventory can be explained by freshwater-seawater mixing. Importantly, however, the deviation towards higher δ^{138}Ba in surface waters and lower δ^{138}Ba in Ba-rich deep-waters cannot be explained by mixing of freshwater and seawater. Instead, Ba removal from well-mixed surface water coupled to Ba recycling in the restricted deep-water and/or mixing of surface water Ba with isotopically light Ba originating from the seafloor must be responsible for the observed trend towards higher Ba concentrations and lower δ^{138}Ba in the deep-water of Kiel Bight (Figure 6C).

5.2 Benthic-pelagic coupling of biogeochemical processes in Kiel Bight

5.2.1 Nutrient and redox cycling

Consistent with long-term observations in Kiel Bight (Lennartz et al., 2014), stratification and intense organic matter export and respiration during the productive season led to low oxygen but high PO_4^{3-} concentrations in the deep-water of Kiel Bight. Nitrate depletion can be explained by denitrification in the oxygen-deficient deep water and/or anoxic surface sediments (Dähnke and Thamdrup, 2013). Anoxic and sulfidic bottom waters were encountered at Station 8 (Figure 2H) whereas at Stations 10 and 13, oxygen was still present in the deep-water (Figure 2C). Due to its restricted location within a local depression (Figure 1), Station 8 is characterized by a shallower pycnocline and deep-water exchange is likely to be limited thus leading to a longer water residence time (i.e., >1 months) (Dietze and Löptien, 2021) and more intense respiration and oxidant drawdown compared to the other stations.

Pore waters in the surface sediments were Fe-rich (ferruginous) at Station 10 but sulfidic throughout the sediment cores at Stations 8 and 13 (Figures 3B, D). Intense organic carbon respiration and opal dissolution in surface sediments released NH_4^+, PO_4^{3-} and SiO_4^{4-} into the pore water (Figures 3E-G). The diffusive flux across the sediment-water interface resulting from nutrient recycling (Table 2) contributed to elevated PO_4^{3-} and SiO_4^{4-} concentrations in the deep-water (Figures 2D, E). The highest flux of NH_4^+, both from greater sediment depth and across the sediment-water interface, was observed at Station 13 within Eckernförde Bay (Figure 3E) indicating that organic carbon degradation was most intense at this site. This notion is consistent with prior studies showing that external nutrient supply and primary productivity decrease from the interior of Eckernförde Bay towards the open Kiel Bight (Maar et al., 2016). The higher benthic phosphate flux observed at Station 10 can be explained by additional PO_4^{3-} release from Fe oxides in the ferruginous surface sediment (Figures 3B, F) (Sundby et al., 1992; Dale et al., 2013). Elevated dissolved Mn concentrations in the anoxic deep-water of Station 8 (Figure 2I) are caused by reductive dissolution of Mn oxides in the surface sediment coupled to Mn diffusion across the sediment-water interface. In contrast, at Stations 10 and 13, where the benthic Mn efflux was similar to or higher than at Station 8 (Figure 2A; Table 2), any Mn liberated into the oxygenated bottom water was readily re-oxidized thus limiting dissolved Mn concentrations in the deep-water (Figure 2I).

5.2.2 Barium cycling and isotope fractionation

The distribution of dissolved Ba and δ^{138}Ba in the water column of Kiel Bight (Figure 5) is generally consistent with that observed in open-ocean settings showing low dissolved Ba concentrations and elevated δ^{138}Ba in the upper water column and high concentrations coupled to low δ^{138}Ba in the deep waters (e.g., Horner et al., 2015; Cao et al., 2016; Bates et al., 2017; Hsieh and Henderson, 2017; Bridgestock et al., 2018; Cao et al., 2020). In the open ocean, this type of Ba distribution has been attributed to barite precipitation within organic

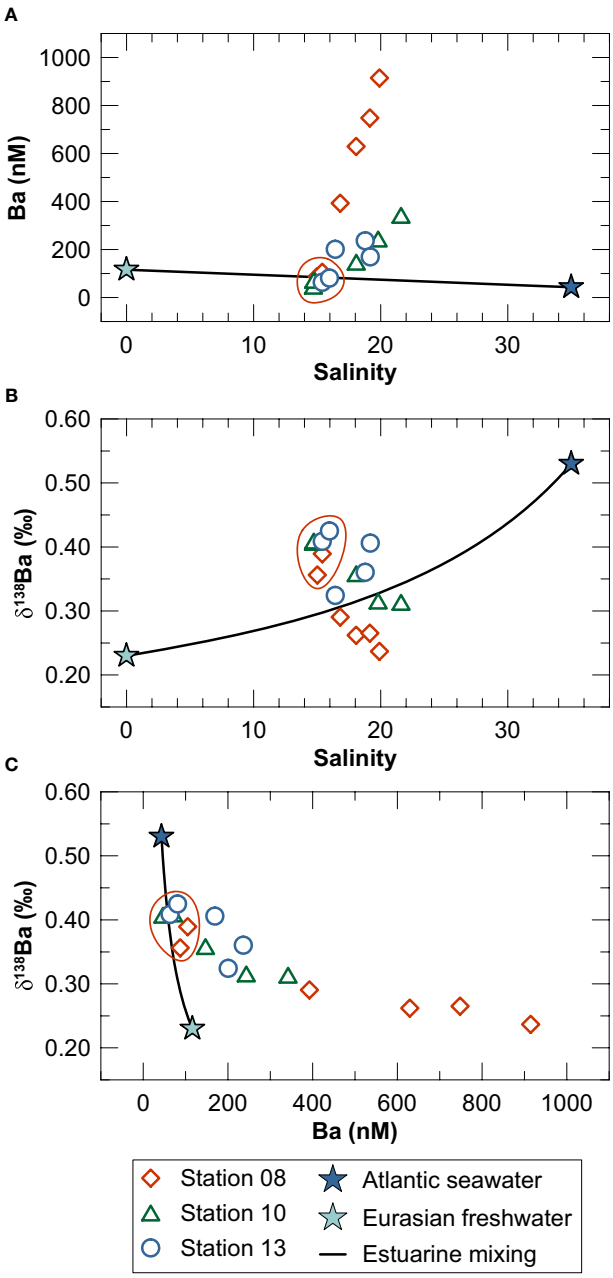

FIGURE 6
Water column data for Kiel Bight in the context of the mixing relationship between freshwater (light blue star) and North Atlantic surface seawater (dark blue star): **(A)** Ba concentration versus salinity, **(B)** δ^{138}Ba versus salinity and **(C)** δ^{138}Ba versus Ba concentration. Endmember values for Eurasian freshwater and North Atlantic surface seawater were taken from Bridgestock et al. (2021b). Red circles depict surface water samples from above the pycnocline.

matter-rich aggregates in the meso-pelagic zone coupled to barite dissolution in undersaturated deep-waters (Church and Wolgemuth, 1972; Dehairs et al., 1980; Bishop, 1988). However, the water column in Kiel Bight is only 20 to 30 m deep. Therefore, the transit time of organic matter-rich particles to the seafloor is rapid compared to open-marine settings. Moreover, the deep-water was oversaturated with respect to barite during sampling (Figure 2K), which is why barite dissolution is unlikely to contribute to the high concentrations of dissolved Ba in the deep-water.

Similar to Mn, PO_4^{3-} and SiO_4^{4-}, dissolved Ba concentrations increased from the bottom water into the pore water and pronounced Ba maxima were observed in the pore water of surface sediments (Figure 5). This observation suggests that the diffusive benthic Ba flux driven by the Ba concentration gradient across the sediment-water interface (Table 2) contributed significantly to high Ba concentrations in the deep-water. Consistent with this interpretation, deep-water samples plot close to barium-rich bottom water and uppermost pore water samples in a mixing plot of δ^{138}Ba versus 1/Ba (Figure 7A). However, the overall relationship between δ^{138}Ba and 1/Ba does not form a linear array indicating that simple two-end member mixing of surface water Ba and sediment-derived Ba is not sufficient to explain the water column Ba concentration and δ^{138}Ba distribution (Figure 7A). Instead, additional isotope fractionation during Ba removal from surface waters and/or mixing of deep-waters and surface water has to be invoked.

Previous studies applied closed-system Rayleigh fractionation (Eq. 7) and open steady-state (Eq. 8) models to evaluate Ba isotope fractionation in marine water columns (e.g., Hsieh and Henderson, 2017; Bridgestock et al., 2018). Closed-system Rayleigh fractionation during Ba removal from surface waters upon upward mixing of deep-water is given by:

$$\delta^{138}Ba_{surface\ water} = \delta^{138}Ba_{deep-water} + 1000 \cdot \left(\frac{1}{\alpha} - 1\right) \cdot \ln F \quad (7)$$

The open steady-state model is described by the following equation:

$$\delta^{138}Ba_{surface\ water} = \delta^{138}Ba_{deep-water} - 1000 \cdot \left(\frac{1}{\alpha} - 1\right) \cdot (1 - F) \quad (8)$$

In Eq.7 and 8, F is the fraction of Ba remaining in the dissolved phase and α is the mass fractionation factor (i.e., the isotope ratio of dissolved Ba divided by the isotope ratio of the particulate Ba phase removed). The best fit to the water column and bottom water data is obtained by the closed-system Rayleigh model applying a mass fractionation factor of +1.000061 (corresponding to a $\Delta^{138}Ba_{dissolved\text{-}particulate}$ of ~+0.061 ‰) (Figure 7B). This isotope fractionation factor is considerably smaller than the one derived from Ba concentration and isotope data for open-marine water columns ($\Delta^{138}Ba_{dissolved\text{-}particulate}$ = ~+0.5), which is thought to reflect Ba isotope fractionation associated with biogenic barite precipitation (Hsieh and Henderson, 2017; Horner and Crockford, 2021). It should be noted, however, that multiple sources contribute to the Ba inventory of Kiel Bight (fresh water, seawater and sediments), which is why application of simple isotope fractionation models might be inappropriate. Regardless of this uncertainty, given that biogenic barite is unlikely to represent the particulate Ba phase forming in the water column of Kiel Bight (see above), another particulate carrier phase for Ba has to be identified.

Potential carrier phases for Ba in marine water columns besides barite include Mn or Fe oxides and organic material (Bishop, 1988; Ganeshram et al., 2003; Sternberg et al., 2005; Gonneea and Paytan, 2006). In the productive summer season (during which our sampling campaign took place), suspended particles in Kiel Bight are predominantly biogenic whereas lithogenic particles are most abundant in late fall and winter when coastal erosion and sediment re-suspension are most intense (Smetacek, 1980). Water column Ba concentrations are well correlated with PO_4^{3-} (Figure 8A). In contrast, the correlation between Ba and SiO_4^{4-} or Mn is weaker and more variable among the three study sites (Figures 8B, C). Furthermore, the correlation between dissolved Ba and Mn does not persist across the

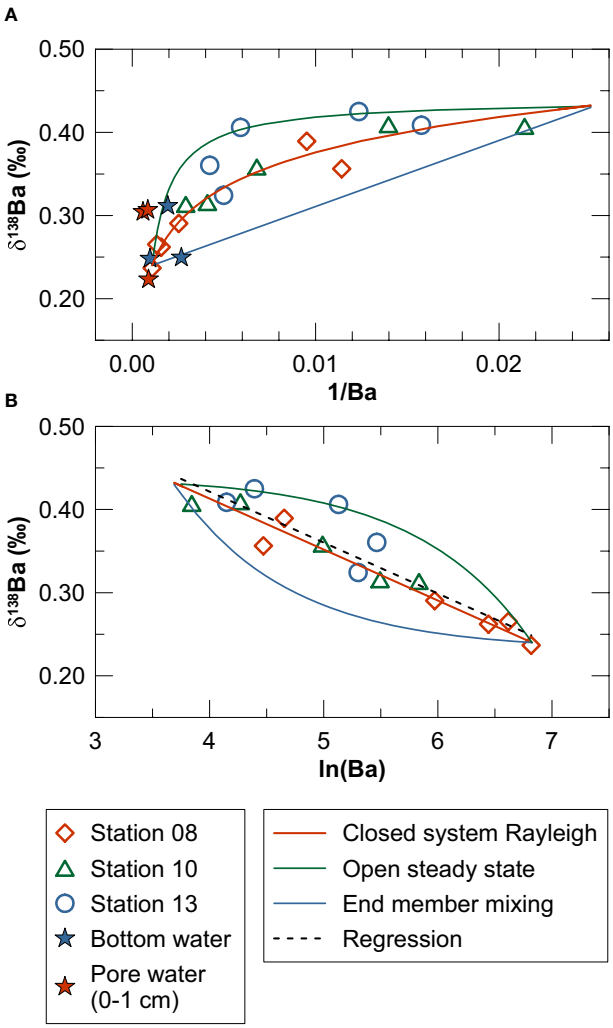

FIGURE 7
Cross plots of **(A)** δ^{138}Ba versus 1/Ba and **(B)** δ^{138}Ba versus ln(Ba) including water column data for Kiel Bight. The mixing plot in **(A)** also contains bottom water and pore water data for MUCs. Solid lines illustrate isotope fractionation during Ba removal from surface waters upon upward mixing of deep-water (closed-system Rayleigh (Eq. 7) and open steady state (Eq. 8) models) as well as conservative end member mixing between deep-water and surface water (calculated analogous to Eq. 5 and 6). The dashed line in **(B)** represents a linear regression through all measured data (δ^{138}Ba = -0.061 · ln(Ba) + 0.667, R^2 = 0.87) illustrating the $\Delta^{138}Ba_{dissolved\text{-}particulate}$ of +0.061 ‰ obtained by the closed-system Rayleigh model.

oxycline (Figure 8C) demonstrating that Mn oxidation and precipitation or another redox-controlled mechanism cannot easily explain Ba removal. Taken together, our data can be best explained by a mechanism in which Ba is removed with biogenic rather than lithogenic particles or Mn oxides. However, the slopes of the Ba to PO_4^{3-} and SiO_4^{4-} relationships (Figures 8A, B) are much steeper than those seen in the open ocean (e.g., Hsieh and Henderson, 2017; Cao et al., 2020), which argues against direct uptake of Ba by phytoplankton with a Redfield-type stoichiometry. Instead, we propose that Ba is passively adsorbed to biogenic particles in the upper water column (cf. Cao et al., 2020) and released into the deep-water and pore water of surface sediments where steep biogeochemical gradients prevail.

5.3 Early diagenetic barium cycling and isotope fractionation

With the exception of the uppermost samples at Stations 8 and 13, sediments in Kiel Bight are characterized by Ba/Al below the local terrigenous background (glacial till at coastal cliffs) (Figures 4B, E, H) indicating that Ba is lost from the terrigenous material upon cliff erosion, sediment transport or diagenesis. The Ba concentrations in the glacial till are higher than those reported for carbonates but generally consistent with those of aluminosilicate minerals (Dehairs et al., 1980; Nan et al., 2018). It is thus possible that Ba is lost from the solid phase due to ion exchange or alteration of aluminosilicate minerals upon contact with seawater. Since the δ^{138}Ba signature of the sediments is, within error, identical to the lithogenic background (Figures 4C, F, I), Ba release from aluminosilicates may contribute to the generally low δ^{138}Ba of brackish water in Kiel Bight compared to open-marine seawater. However, the isotope composition of the terrigenous Ba (~±0.0 ‰) is too low to exclusively explain the δ^{138}Ba of deep-waters and pore waters of surface sediments (~+0.25 ‰). Furthermore, as demonstrated in Section 5.2.2, simple mixing of sediment-derived Ba (e.g., from aluminosilicate minerals) and seawater Ba cannot explain the Ba versus δ^{138}Ba relationship in the water column (Figure 7).

The highest dissolved Ba concentrations are observed in the pore water of the uppermost 1 or 2 cm of the sediment (Figure 5) and the concentration gradient between surface sediments and bottom waters drives a diffusive Ba flux across the sediment-water interface. As demonstrated above, this efflux contributed to the relatively light isotopic signature of the bottom water (Figures 5, 7A). High dissolved Ba concentrations within the pore water of surface sediments coincided with low solid phase total Ba concentrations but elevated Ba/Al (above the local terrigenous background at Stations 8 and 13) and TOC (Figures 4B, E, H). This observation indicates that both non-lithogenic Ba and fresh organic material are present within the uppermost sediment layer. Furthermore, intense remineralization of fresh organic material also occurs within the uppermost 1 - 2 cm of the sediment (Dale et al., 2013; Perner et al., 2022), which can explain Ba release into the pore water (Figure 4).

We do not observe a correlation between pore water Ba and the major nutrients PO_4^{3-}, SiO_4^{4-} and NH_4^+. However, such a correlation is not expected given that below the surface sediments (>1 - 2 cm), nutrient and Ba profiles are governed by different processes: PO_4^{3-}, NH_4^+ and SiO_4^{4-} concentrations continue to increase (Figures 3E-G) due to remineralization of refractory organic matter (Dale et al., 2013; Perner et al., 2022) and opal dissolution, respectively. In contrast, dissolved Ba concentrations decrease and approach equilibrium with respect to barite (Figures 3H, I). This observation suggests that Ba is precipitated as authigenic barite. In subsurface sediments, pore water and solid phase are in continuous contact, which is why dissolved Ba is more likely to reach thermodynamic equilibrium with respect to barite compared to the shallow water column of Kiel Bight. Below 18 cm sediment depth at Station 13, the pore water became undersaturated with respect to barite and dissolved Ba concentrations increased again (Figures 3H, I). This shift in saturation state was related to intense organic carbon degradation by sulfate reduction causing near-complete depletion of sulfate within the recovered sediment interval at this site (Figures 3C-E). Increasing concentrations of Ba in the pore water are thus attributed to well-known barite dissolution in the sulfate-methane transition zone (Torres et al., 1996; Riedinger et al., 2006).

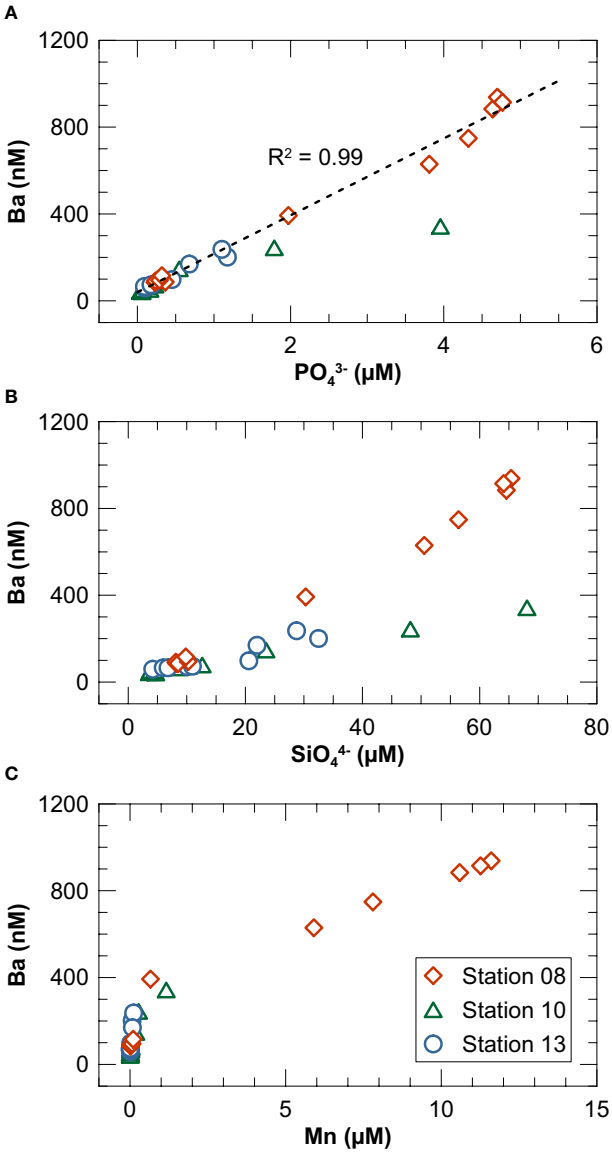

FIGURE 8
Cross plots of dissolved Ba concentrations in the water column versus **(A)** PO_4^{3-}, **(B)** SiO_4^{4-} and **(C)** Mn. The dashed line in **(A)** represents a linear regression through all data.

In contrast to the water column in Kiel Bight and the open ocean (Horner and Crockford, 2021), pore water Ba concentrations and δ^{138}Ba in subsurface sediments do not show a mirror image but are correlated, i.e., low Ba concentrations (coinciding with SI_{barite} = ~0) are accompanied by low δ^{138}Ba whereas high Ba concentrations (coinciding with SI_{barite} < 0) are accompanied by high δ^{138}Ba (Figure 5). This observation implies that authigenic barite precipitation at all our sites preferentially removes the heavy Ba isotopes and barite dissolution returns this heavy isotope signature back to solution (Station 13). Importantly, this finding is in apparent conflict with the results of barite precipitation experiments and water column studies showing that the light Ba isotopes are preferentially incorporated into the solid (von Allmen et al., 2010; Horner et al., 2017; Crockford et al., 2019). We note, however, that Ba isotope fraction during barite precipitation from pore water has not been studied to date. Moreover, the thermodynamic and/or kinetic circumstances of Ba isotope fractionation in sediments, suspended particles and laboratory experiments are likely to differ substantially, which is why differing extents and directions of isotope fractionation are conceivable. Different $\Delta^{138}Ba_{seawater\text{-}barite}$ obtained in experiments (~+0.3 ‰) and inferred from water column data (~+0.5 ‰) (Horner and Crockford, 2021) may also reflect differing environmental conditions during barium isotope fractionation. Support for our finding of a relatively heavy δ^{138}Ba in authigenic barite comes from a recent study about Black Shale weathering (Charbonnier et al., 2022). These authors demonstrated that weathering of organic carbon-rich sedimentary rocks mobilized Ba with a relatively heavy δ^{138}Ba compared to siliciclastic material.

6 Conclusion

The inventory and isotope composition of dissolved Ba in Kiel Bight can broadly be explained by mixing of freshwater and North Atlantic seawater. In addition, vertical profiles of dissolved Ba concentrations and δ^{138}Ba in the water column and sediments reflect a close coupling of pelagic and benthic Ba cycling processes. Removal of dissolved Ba from surface waters preferentially transfers the light Ba isotopes to the deep-water and surface sediments. Release of this light Ba to the pore waters of surface sediments drives a flux of isotopically light Ba across the sediment-water interface into the deep-waters. Precipitation and re-dissolution of biogenic barite cannot explain these trends because barite is strongly oversaturated in the deep-waters and surface sediments. Co-variation of dissolved Ba in the water column with nutrient concentrations suggests that Ba removal is primarily mediated by adsorption to biogenic particles and recycling is coupled to the remineralization of fresh organic material close to the sediment-water interface. We argue that mechanisms of Ba removal and recycling observed in Kiel Bight may also operate in other marine systems. However, in open-marine environments with a deeper water column, a higher proportion of the Ba recycling from biogenic particles is likely to happen in the water column (rather than in the sediments) and the Ba released may contribute to biogenic barite precipitation. Taking into account this additional process could help to explain some of the mismatch between $\Delta^{138}Ba_{seawater\text{-}barite}$ values inferred from experiments and water column data.

Pore water data for subsurface sediments in Kiel Bight indicate preferential removal of isotopically heavy Ba into the sediment solid phase (presumably into authigenic barite) during early diagenesis. Even though some of this heavy Ba may be recycled into the pore water upon sulfate depletion, diffusive loss of Ba from subsurface sediments is impeded by the downward concentration gradient prevailing above. Burial of isotopically heavy Ba with authigenic barite (or another, yet unidentified particulate Ba phase) in continental margin sediments could potentially help to settle the isotopic imbalance between known Ba source and sink fluxes in the ocean.

Our data from Kiel Bight demonstrate that sedimentary processes and benthic fluxes can have a strong influence on the Ba concentration and isotope composition of coastal and near bottom seawater. More research on Ba isotope fractionation processes during water-sediment interactions in various seafloor environments is required to incorporate those processes and fluxes in the global ocean's Ba isotope budget.

Data availability statement

The data reported in this article are available at PANGAEA (https://doi.pangaea.de/10.1594/PANGAEA.954246).

Author contributions

FS designed the study, lead the research cruise, interpreted data and wrote the manuscript. JC measured data, contributed to data interpretation and manuscript writing. ZZ measured data, contributed to data interpretation and manuscript writing. PV measured data and contributed to manuscript writing. CS contributed to data interpretation and manuscript writing. MF contributed to data interpretation and manuscript writing. All authors contributed to the article and approved the submitted version.

Funding

This work was supported by the German Research Foundation (DFG) through Emmy Noether Research Group ICONOX (Iron Cycling in Continental Margin Sediments and the Nutrient and Oxygen Balance of the Ocean). The China Scholarship Council (CSC) supported JC during his stay in Kiel.

Acknowledgments

We would like to thank the crew of RV Alkor during Cruise AL543 for their commitment during the sampling campaign as well as the GEOMAR technicians Anke Bleyer, Anna-Kathrin Retschko, Kastriot Qelaj and Regina Surberg for support in the laboratory. Helpful comments by two reviewers are gratefully acknowledged.

Conflict of interest

The authors declare that the research was conducted in the absence of any commercial or financial relationships that could be construed as a potential conflict of interest.

Publisher's note

References

Averes, T., Hofstede, J. L. A., Hinrichsen, A., Reimers, H.-C., and Winter, C. (2021). Cliff retreat contribution to the littoral sediment budget along the Baltic Sea coastline of schleswig-Holstein, Germany. *J. Mar. Sci. Eng.* 9, 870. doi: 10.3390/jmse9080870

Bates, S. L., Hendry, K. R., Pryer, H. V., Kinsley, C. W., Pyle, K. M., Woodward, E. M. S., et al. (2017). Barium isotopes reveal role of ocean circulation on barium cycling in the Atlantic. *Geochim. Cosmochim. Acta* 204, 286–299. doi: 10.1016/j.gca.2017.01.043

Bishop, J. K. B. (1988). The barite-opal-organic carbon association in oceanic particulate matter. *Nature* 332, 341–343. doi: 10.1038/332341a0

Boudreau, B. P. (1996). The diffusive tortuosity of fine-grained unlithified sediments. *Geochim. Cosmochim. Acta* 60, 3139–3142. doi: 10.1016/0016-7037(96)00158-5

Bridgestock, L., Hsieh, Y.-T., Porcelli, D., Homoky, W. B., Bryan, A., and Henderson, G. M. (2018). Controls on the barium isotope compositions of marine sediments. *Earth Planet. Sci. Lett.* 481, 101–110. doi: 10.1016/j.epsl.2017.10.019

Bridgestock, L., Nathan, J., Hsieh, Y.-T., Holdship, P., Porcelli, D., Andersson, P. S., et al. (2021b). Assessing the utility of barium isotopes to trace Eurasian riverine freshwater inputs to the Arctic ocean. *Mar. Chem.* 236, 104029. doi: 10.1016/j.marchem.2021.104029

Bridgestock, L., Nathan, J., Paver, R., Hsieh, Y.-T., Porcelli, D., Tanzil, J., et al. (2021a). Estuarine processes modify the isotope composition of dissolved riverine barium fluxes to the ocean. *Chem. Geol.* 579, 120340. doi: 10.1016/j.chemgeo.2021.120340

Cao, Z., Li, Y., Rao, X., Yu, Y., Hathorne, E. C., Siebert, C., et al. (2020). Constraining barium isotope fractionation in the upper water column of the south China Sea. *Geochim. Cosmochim. Acta* 288, 120–137. doi: 10.1016/j.gca.2020.08.008

Cao, Z., Rao, X., Yu, Y., Siebert, C., Hathorne, E. C., Liu, B., et al. (2021). Stable barium isotope dynamics during estuarine mixing. *Geophys. Res. Lett.* 48, e2021GL095680. doi: 10.1029/2021GL095680

Cao, Z., Siebert, C., Hathorne, E. C., Dai, M., and Frank, M. (2016). Constraining the oceanic barium cycle with stable barium isotopes. *Earth Planet. Sci. Lett.* 434, 1–9. doi: 10.1016/j.epsl.2015.11.017

Chan, L. H., Drummond, D., Edmond, J. M., and Grant, B. (1977). On the barium data from the Atlantic GEOSECS expedition. *Deep Sea Res.* 24, 613–649. doi: 10.1016/0146-6291(77)90505-7

Charbonnier, Q., Bouchez, J., Gaillardet, J., Calmels, D., and Dellinger, M. (2022). The influence of black shale weathering on riverine barium isotopes. *Chem. Geol.* 594, 120741. doi: 10.1016/j.chemgeo.2022.120741

Church, T. M., and Wolgemuth, K. (1972). Marine barite saturation. *Earth Planet. Sci. Lett.* 15, 35–44. doi: 10.1016/0012-821X(72)90026-X

Coffey, M., Dehairs, F., Collette, O., Luther, G., Church, T., and Jickells, T. (1997). The behaviour of dissolved barium in estuaries. *Estuar. Coast. Shelf Sci.* 45, 113–121. doi: 10.1006/ecss.1996.0157

Crockford, P. W., Wing, B. A., Paytan, A., Hodgskiss, M. S. W., Mayfield, K. K., Hayles, J. A., et al. (2019). Barium-isotopic constraints on the origin of post-marinoan barites. *Earth Planet. Sci. Lett.* 519, 234–244. doi: 10.1016/j.epsl.2019.05.018

Dähnke, K., and Thamdrup, B. (2013). Nitrogen isotope dynamics and fractionation during sedimentary denitrification in boknis eck, Baltic Sea. *Biogeosciences* 10, 3079–3088. doi: 10.5194/bg-10-3079-2013

Dale, A. W., Bertics, V. J., Treude, T., Sommer, S., and Wallmann, K. (2013). Modeling benthic-pelagic nutrient exchange processes and porewater distributions in a seasonally hypoxic sediment: evidence for massive phosphate release by beggiatoa? *Biogeosciences* 10, 629–651. doi: 10.5194/bg-10-629-2013

Dehairs, F., Chesselet, R., and Jedwab, J. (1980). Discrete suspended particles of barite and the barium cycle in the open ocean. *Earth Planet. Sci. Lett.* 49, 528–550. doi: 10.1016/0012-821X(80)90094-1

Dellwig, O., Schnetger, B., Meyer, D., Pollehne, F., Häusler, K., and Arz, H. W. (2018). Impact of the major Baltic inflow in 2014 on manganese cycling in the gotland deep (Baltic Sea). *Front. Mar. Sci.* 5. doi: 10.3389/fmars.2018.00248

Dietze, H., and Löptien, U. (2021). Retracing hypoxia in eckernförde bight (Baltic Sea). *Biogeosciences* 18, 4243–4264. doi: 10.5194/bg-18-4243-2021

Dymond, J., and Collier, R. (1996). Particulate barium fluxes and their relationships to biological productivity. *Deep Sea Res. Part II: Topical Stud. Oceanogr.* 43, 1283–1308. doi: 10.1016/0967-0645(96)00011-2

Dymond, J., Suess, E., and Lyle, M. (1992). Barium in deep-Sea sediment: A geochemical proxy for paleoproductivity. *Paleoceanography* 7, 163–181. doi: 10.1029/92PA00181

Elderfield, H., and Schultz, A. (1996). Mid-ocean ridge hydrothermal fluxes and the chemical composition of the ocean. *Annu. Rev. Earth Planet. Sci.* 24, 191–224. doi: 10.1146/annurev.earth.24.1.191

Fisher, N. S., Guillard, R. R., and Bankston, D. C. (1991). The accumulation of barium by marine phytoplankton grown in culture. *J. Mar. Res.* 49, 339–354.

Ganeshram, R. S., François, R., Commeau, J., and Brown-Leger, S. L. (2003). An experimental investigation of barite formation in seawater. *Geochim. Cosmochim. Acta* 67, 2599–2605. doi: 10.1016/S0016-7037(03)00164-9

Geyman, B. M., Ptacek, J. L., Lavigne, M., and Horner, T. J. (2019). Barium in deep-sea bamboo corals: Phase associations, barium stable isotopes, & prospects for paleoceanography. *Earth Planet. Sci. Lett.* 525, 115751. doi: 10.1016/j.epsl.2019.115751

Gong, Y., Zeng, Z., Cheng, W., Lu, Y., Zhang, L., Yu, H., et al. (2020). Barium isotopic fractionation during strong weathering of basalt in a tropical climate. *Environ. Int.* 143, 105896. doi: 10.1016/j.envint.2020.105896

Gonneea, M. E., and Paytan, A. (2006). Phase associations of barium in marine sediments. *Mar. Chem.* 100, 124–135. doi: 10.1016/j.marchem.2005.12.003

Grasshoff, K., Erhardt, M., and Kremling, K. (1999). *Methods of seawater analysis* (Weinheim: Wiley-VCH).

Gruber, N., and Sarmiento, J. L. (1997). Global patterns of marine nitrogen fixation and denitrification. *Global Biogeochem. Cycles* 11, 235–266. doi: 10.1029/97GB00077

Hanor, J. S., and Chan, L.-H. (1977). Non-conservative behavior of barium during mixing of Mississippi river and gulf of Mexico waters. *Earth Planet. Sci. Lett.* 37, 242–250. doi: 10.1016/0012-821X(77)90169-8

Horner, T., and Crockford, P. (2021). Barium isotopes: Drivers, dependencies, and distributions through space and time. *(Elements in Geochemical Tracers in Earth System Science)* Cambridge: Cambridge University Press. doi: 10.1017/9781108865845

Horner, T. J., Kinsley, C. W., and Nielsen, S. G. (2015). Barium-isotopic fractionation in seawater mediated by barite cycling and oceanic circulation. *Earth Planet. Sci. Lett.* 430, 511–522. doi: 10.1016/j.epsl.2015.07.027

Horner, T. J., Pryer, H. V., Nielsen, S. G., Crockford, P. W., Gauglitz, J. M., Wing, B. A., et al. (2017). Pelagic barite precipitation at micromolar ambient sulfate. *Nat. Commun.* 8, 1342. doi: 10.1038/s41467-017-01229-5

Hsieh, Y.-T., and Henderson, G. M. (2017). Barium stable isotopes in the global ocean: Tracer of ba inputs and utilization. *Earth Planet. Sci. Lett.* 473, 269–278. doi: 10.1016/j.epsl.2017.06.024

Lehmann, A., and Myrberg, K. (2008). Upwelling in the Baltic Sea — a review. *J. Mar. Syst.* 74, S3–S12. doi: 10.1016/j.jmarsys.2008.02.010

Lennartz, S. T., Lehmann, A., Herrford, J., Malien, F., Hansen, H. P., Biester, H., et al. (2014). Long-term trends at the boknis eck time series station (Baltic Sea), 1957-2013: does climate change counteract the decline in eutrophication? *Biogeosciences* 11, 6323–6339. doi: 10.5194/bg-11-6323-2014

Li, Y.-H., and Gregory, S. (1974). Diffusion of ions in sea water and in deep-sea sediments. *Geochim. Cosmochim. Acta* 38, 703–714. doi: 10.1016/0016-7037(74)90145-8

Maar, M., Markager, S., Madsen, K. S., Windolf, J., Lyngsgaard, M. M., Andersen, H. E., et al. (2016). The importance of local versus external nutrient loads for chl a and primary production in the Western Baltic Sea. *Ecol. Model.* 320, 258–272. doi: 10.1016/j.ecolmodel.2015.09.023

Martinez-Ruiz, F., Jroundi, F., Paytan, A., Guerra-Tschuschke, I., Abad, M. D. M., and González-Muñoz, M. T. (2018). Barium bioaccumulation by bacterial biofilms and implications for ba cycling and use of ba proxies. *Nat. Commun.* R. Feistel, G. Nausch and N. Wasmund (Eds) 9, 1619. doi: 10.1038/s41467-018-04069-z

Matthäus, W., Nehring, D., Feistel, R., Nausch, G., Mohrholz, V., and Lass, H.-U. (2008). "The inflow of highly saline water into the Baltic Sea," in *State and evolution of the Baltic Sea 1952–2005*, 265–309.

McManus, J., Berelson, W. M., Klinkhammer, G. P., Johnson, K. S., Coale, K. H., Anderson, R. F., et al. (1998). Geochemistry of barium in marine sediments: implications for its use as a paleoproxy. *Geochim. Cosmochim. Acta* 62, 3453–3473. doi: 10.1016/S0016-7037(98)00248-8

McManus, J., Berelson, W. M., Klinkhammer, G. P., Kilgore, T. E., and Hammond, D. E. (1994). Remobilization of barium in continental margin sediments. *Geochim. Cosmochim. Acta* 58, 4899–4907. doi: 10.1016/0016-7037(94)90220-8

Mohrholz, V. (2018). Major Baltic inflow statistics – revised. *Front. Mar. Sci.* 5. doi: 10.3389/fmars.2018.00384

Mohrholz, V., Naumann, M., Nausch, G., Krüger, S., and Gräwe, U. (2015). Fresh oxygen for the Baltic Sea — an exceptional saline inflow after a decade of stagnation. *J. Mar. Syst.* 148, 152–166. doi: 10.1016/j.jmarsys.2015.03.005

Nan, X.-Y., Yu, H.-M., Rudnick, R. L., Gaschnig, R. M., Xu, J., Li, W.-Y., et al. (2018). Barium isotopic composition of the upper continental crust. *Geochim. Cosmochim. Acta* 233, 33–49. doi: 10.1016/j.gca.2018.05.004

Nürnberg, C. C., Bohrmann, G., Schlüter, M., and Frank, M. (1997). Barium accumulation in the Atlantic sector of the southern ocean: Results from 190,000-year records. *Paleoceanography* 12, 594–603. doi: 10.1029/97PA01130

Paytan, A., and Griffith, E. M. (2007). Marine barite: Recorder of variations in ocean export productivity. *Deep Sea Res. Part II: Topical Stud. Oceanogr.* 54, 687–705. doi: 10.1016/j.dsr2.2007.01.007

Paytan, A., and Kastner, M. (1996). Benthic ba fluxes in the central equatorial pacific, implications for the oceanic ba cycle. *Earth Planet. Sci. Lett.* 142, 439–450. doi: 10.1016/0012-821X(96)00120-3

Paytan, A., Kastner, M., and Chavez, F. P. (1996). Glacial to interglacial fluctuations in productivity in the equatorial pacific as indicated by marine barite. *Science* 274, 1355–1357. doi: 10.1126/science.274.5291.1355

Parkhurst, D. L., and Appelo, C. A. J. (2013). "One-dimensional transport, and inverse geochemical calculations. US geological survey techniques and methods, book 6, chapter A43," in *Description of input and examples for PHREEQC version 3–a computer program for speciation, batch-reaction*, 497. Available at: http://pubs.usgs.gov/tm/06/a43.

Plass, A., Retschko, A. K., Türk, M., Fischer, T., and Scholz, F. (2022). A novel device for trace metal-clean sampling of bottom water and suspended particles at the ocean's lower boundary: The benthic trace profiler. *Limnology Oceanography: Methods* 20, 102–114.

Perner, M., Wallmann, K., Adam-Beyer, N., Hepach, H., Laufer-Meiser, K., Böhnke, S., et al. (2022). Environmental changes affect the microbial release of hydrogen sulfide and methane from sediments at boknis eck (SW Baltic Sea). *Front. Microbiol.* 13. doi: 10.3389/fmicb.2022.1096062

Rahman, S., Shiller, A. M., Anderson, R. F., Charette, M. A., Hayes, C. T., Gilbert, M., et al. (2022). Dissolved and particulate barium distributions along the US GEOTRACES north Atlantic and East pacific zonal transects (GA03 and GP16): Global implications for the marine barium cycle. *Global Biogeochem. Cycles* 36, e2022GB007330. doi: 10.1029/2022GB007330

Riedinger, N., Kasten, S., Gröger, J., Franke, C., and Pfeifer, K. (2006). Active and buried authigenic barite fronts in sediments from the Eastern cape basin. *Earth Planet. Sci. Lett.* 241, 876–887. doi: 10.1016/j.epsl.2005.10.032

Scholz, F., Baum, M., Siebert, C., Eroglu, S., Dale, A. W., Naumann, M., et al. (2018). Sedimentary molybdenum cycling in the aftermath of seawater inflow to the intermittently euxinic gotland deep, central Baltic Sea. *Chem. Geol.* 491, 27–38. doi: 10.1016/j.chemgeo.2018.04.031

Scholz, F., Hensen, C., Noffke, A., Rohde, A., Liebetrau, V., and Wallmann, K. (2011). Early diagenesis of redox-sensitive trace metals in the Peru upwelling area – response to ENSO-related oxygen fluctuations in the water column. *Geochim. Cosmochim. Acta* 75, 7257–7276. doi: 10.1016/j.gca.2011.08.007

Schulz, H. D. (2006). "Quantification of early diagenesis: Dissolved constituents in pore water and signals in the solid phase," in *Marine geochemistry, 2nd revised ed*. Eds. H. D. Schulz and M. Zabel (Berlin: Springer), 75–121.

Seibold, E., Exon, N., Hartmann, M., Kögler, F.-C., Krumm, H., Lutze, G., et al. (1971). "Marine geology of Kiel bay," in *Sedimentology of Parts of Central Europe, Guidebook VIII* (Heidelberg, Germany: International Sedimentology Congress) pp. 209-235.

Siebert, C., Nägler, T. F., and Kramers, J. D. C. (2001). Determination of molybdenum isotope fractionation by double-spike multicollector inductively coupled plasma mass spectrometry. *Geochemistry Geophysics Geosystems* 2. doi: 10.1029/2000GC000124

Shaw, T. J., Moore, W. S., Kloepfer, J., and Sochaski, M. A. (1998). The flux of barium to the coastal waters of the southeastern USA: the importance of submarine groundwater discharge. *Geochim. Cosmochim. Acta* 62, 3047–3054. doi: 10.1016/S0016-7037(98)00218-X

Smetacek, V. (1980). Annual cycle of sedimentation in relation to plankton ecology in western Kiel bight. *Ophelia* Suppl. 1, 65–76.

Sternberg, E., Tang, D., Ho, T.-Y., Jeandel, C., and Morel, F. M. M. (2005). Barium uptake and adsorption in diatoms. *Geochim. Cosmochim. Acta* 69, 2745–2752. doi: 10.1016/j.gca.2004.11.026

Stookey, L. L. (1970). Ferrozine - a new spectrophotometric reagent for iron. *Anal. Chem.* 42, 779–781. doi: 10.1021/ac60289a016

Sundby, B. R., Gobeil, C., Silverberg, N., and Alfonso, M. (1992). The phosphorus cycle in coastal marine sediments. *Limnol. Oceanogr.* 37, 1129–1145. doi: 10.4319/lo.1992.37.6.1129

Torres, M. E., Brumsack, H. J., Bohrmann, G., and Emeis, K. C. (1996). Barite fronts in continental margin sediments: a new look at barium remobilization in the zone of sulfate reduction and formation of heavy barites in diagenetic fronts. *Chem. Geol.* 127, 125–139. doi: 10.1016/0009-2541(95)00090-9

von Allmen, K., Böttcher, M. E., Samankassou, E., and Nägler, T. F. (2010). Barium isotope fractionation in the global barium cycle: First evidence from barium minerals and precipitation experiments. *Chem. Geol.* 277, 70–77. doi: 10.1016/j.chemgeo.2010.07.011

Wallmann, K., Diesing, M., Scholz, F., Rehder, G., Dale, A. W., Fuhr, M., et al. (2022). Erosion of carbonate-bearing sedimentary rocks may close the alkalinity budget of the Baltic Sea and support atmospheric CO2 uptake in coastal seas. *Front. Mar. Sci.* 9. doi: 10.3389/fmars.2022.968069

Wasmund, N., Göbel, J., and Bodungen, B. V. (2008). 100-years-changes in the phytoplankton community of Kiel bight (Baltic Sea). *J. Mar. Syst.* 73, 300–322. doi: 10.1016/j.jmarsys.2006.09.009

Whitmore, L. M., Shiller, A. M., Horner, T. J., Xiang, Y., Auro, M. E., Bauch, D., et al. (2022). Strong margin influence on the Arctic ocean barium cycle revealed by pan-Arctic synthesis. *J. Geophys. Res.: Oceans* 127, e2021JC017417. doi: 10.1029/2021JC017417

Yu, Y., Hathorne, E., Siebert, C., Felis, T., Rajendran, C. P., and Frank, M. (2022). Monthly resolved coral barium isotopes record increased riverine inputs during the south Asian summer monsoon. *Geochim. Cosmochim. Acta* 329, 152–167. doi: 10.1016/j.gca.2022.05.001

Yu, Y., Siebert, C., Fietzke, J., Goepfert, T., Hathorne, E., Cao, Z., et al. (2020). The impact of MC-ICP-MS plasma conditions on the accuracy and precision of stable isotope measurements evaluated for barium isotopes. *Chem. Geol.* 549, 119697. doi: 10.1016/j.chemgeo.2020.119697